Replacing bulk Pt in Pt–Ni–Pt bimetallic structures with tungsten monocarbide (WC): Hydrogen adsorption and cyclohexene hydrogenation on Pt–Ni–WC

Michael P. Humbert, Carl A. Menning, Jingguang G. Chen *

Department of Chemical Engineering, Center for Catalytic Science and Technology (CCST), University of Delaware, Newark, DE 19716, USA

ARTICLE INFO

ABSTRACT

It is well known that bimetallic surfaces, such as the Pt–Ni–Pt(bulk) structure, with one monolayer of Ni residing in the subsurface region of Pt, often show unique catalytic properties including low temperature hydrogenation pathways. It is also known that transition metal carbides, such as tungsten monocarbide (WC), often show catalytic properties similar to Pt. In the current study, we explored the possibility to replace bulk Pt in the Pt–Ni–Pt(bulk) structure by anchoring Pt–Ni on a WC substrate. The dissociative adsorption of hydrogen and the hydrogenation of cyclohexene were used as probe reactions to evaluate the chemical properties of Pt–Ni–WC(bulk), with Density Functional Theory (DFT) calculations and Temperature Programmed Desorption (TPD) measurements being performed. Similar to Pt–Ni–Pt, the Pt–Ni–WC surface shows weakly bonded hydrogen as predicted from DFT calculations and confirmed by TPD experiments. In addition, the presence of weakly bonded atomic hydrogen and cyclohexene led to the low temperature hydrogenation of cyclohexene, again similar to that observed on Pt–Ni–Pt. Our results indicate that anchoring the Pt–Ni structure on WC should potentially reduce the loading of Pt in the bimetallic catalysts. Furthermore, the replacement of bulk Pt by WC should also prevent the diffusion of the subsurface Ni into the bulk, potentially increasing the stability of the desirable subsurface bimetallic structure in Pt–Ni–WC.

1. Introduction

Pt catalysts are widely used due to their ability to facilitate a wide array of chemical reactions such as petroleum cracking, hydrogenation, the oxidation of carbon monoxide in automobile catalytic converters, and the oxidation and reduction reactions in polymer electrolyte membrane (PEM) fuel cells [1–10]. Despite their diverse catalytic applications, the widespread use of Pt catalysts is often limited by the high cost and limited supply of the precious metal. To overcome this, Pt is often modified with some other metal to enhance the activity and/or selectivity of the catalyst, thus decreasing the Pt loading needed to carry out the desired reaction. A substantial amount of experimental and theoretical research has been conducted to determine the origins of the improved catalytic properties of Pt-based bimetallic catalysts [1–10]. While a fundamental understanding is beginning to take shape, it is also becoming apparent that there are several key issues with the use of Pt-based bimetallic catalysts. Despite gains in activity and/or selectivity, bimetallic catalysts are susceptible to many modes of deactivation. In addition to poisoning by adsorbates, coking, and sintering, bimetallic catalysts can also undergo deactivation if the unique structures of their bimetallic bonding are compromised [1–4].

One family of Pt-based catalysts that has received considerable attention is Pt modified by 3d transition metals [9,11–16]. These catalysts have exhibited improvements in the activity and/or selectivity of the hydrogenation of alkenes and α,β-unsaturated aldehydes [9,13], the reforming of oxygenates [14,15], and in the oxygen reduction reaction in PEM fuel cells [16]. Of the 3d transition metals, Ni modification of Pt has been shown to result in the highest activity and selectivity for hydrogenation reactions on both model surfaces and supported catalysts [6,13,17–19] and thus will be the focus of the current paper.

Previous surface science studies have revealed that different bimetallic configurations can be synthesized when Ni is deposited onto Pt(1 1 1). If the deposition is performed at room temperature Ni atoms remain on top of Pt, resulting in a surface configuration, Ni–Pt–Pt(1 1 1). At elevated temperatures, Ni will diffuse into the bulk. However, if the temperature is kept at an intermediate range of ~600 to ~800 K, a subsurface configuration, Pt–Ni–Pt(1 1 1), with the topmost atomic layer enriched in Pt and the second layer enriched in Ni, is produced. Due to both surface strain and heterometallic bonding interactions, or the ligand effect, these two types of bimetallic surfaces have distinct surface electronic properties [7], leading to different binding strength of adsorbates and thus different catalytic properties.

The bimetallic structure of interest in the current manuscript is the Pt–Ni–Pt(1 1 1) subsurface configuration which, in comparison

* Corresponding author. Fax: +1 302 831 2085.
E-mail address: jgchen@udel.edu (J.G. Chen).

with Pt(1 1 1), has favorable catalytic properties to enhance the activity and selectivity of the hydrogenation of small unsaturated hydrocarbons [17,20]. Specifically, this subsurface structure has a d-band center that is shifted away from the Fermi level in comparison with Pt(1 1 1), resulting in weaker binding of atomic hydrogen and alkenes. For example, while Pt(1 1 1) binds cyclohexene strongly enough to favor dehydrogenation and decomposition, Pt–Ni–Pt(1 1 1) binds cyclohexene strongly enough to undergo hydrogenation, but not too strongly so that the extent of dehydrogenation and decomposition is reduced [13].

These enhanced catalytic properties are only realized on the subsurface Pt–Ni–Pt(1 1 1) configuration. If elevated temperatures are required for reaction, the Ni atoms no longer reside in the second layer of Pt(1 1 1), but instead diffuse into the bulk leaving a monometallic Pt(1 1 1) surface. Also, adsorbates such as oxygen can cause the subsurface Ni atoms to segregate to the surface, forming the Ni–Pt–Pt(1 1 1) surface, which favors the undesired decomposition and dehydrogenation over hydrogenation [13]. As tungsten monocarbide (WC) has been shown to demonstrate catalytic properties similar to Pt [21–23], one idea to overcome the inherent instability of Pt–Ni–Pt(1 1 1) is to replace the bulk Pt with WC to produce the Pt–Ni–WC structure. Another reason for choosing the WC substrate as a model surface for transition metal carbides is because of its relatively high stability in air, as demonstrated previously in the comparative studies between WC and W₂C [23]. In addition, as WC has been shown to be an effective diffusion barrier layer to prevent the inward diffusion of metal overlayers [24], thermal deactivation due to Ni diffusion will be alleviated. Furthermore, it is possible that the WC will anchor Ni by the formation of W–Ni or C–Ni bonds to prevent its segregation to the surface in an oxygen-rich environment. Ultimately, a highly active and more stable catalyst that utilizes far less Pt may be realized by anchoring the Pt–Ni bimetallic structure on the WC substrate.

In this paper, surface science experiments are performed on a polycrystalline W foil substrate to examine the feasibility of replacing the bulk Pt of the Pt–Ni–Pt(1 1 1) surface with WC. This is accomplished by carburizing the W foil followed by subsequent deposition of a monolayer of Ni and Pt. Upon annealing the Pt–Ni-modified WC surface, it is expected that the first atomic layer will be enriched in Pt due to the enthalpic driving force created by the lower surface energy of Pt in comparison with the Ni [25]. Strain will also assist in driving the Pt to the surface as elastic strain is reduced by having the larger Pt atoms in the topmost atomic layer.

In order to probe the chemical properties of the Pt–Ni–WC surface, the dissociative adsorption of hydrogen is used as a probe reaction to determine whether the hydrogen binding energy on Pt–Ni–WC is similar to Pt–Ni–Pt. Cyclohexene is also used as a probe molecule because cyclic hydrocarbons are important reaction intermediates in many refinery and petrochemical processes, in addition to serving as building blocks for many chemicals produced in the chemical industry. In addition, cyclohexene has several competitive reaction pathways including decomposition, dehydrogenation, disproportionation, and hydrogenation. The hydrogenation pathway is of particular interest in this study as Pt–Ni–Pt(1 1 1) has shown a unique low temperature hydrogenation pathway to produce cyclohexane [13].

2. Experimental and DFT methods

2.1. Preparation of WC surface

All experiments were performed in a two-level stainless steel ultra-high vacuum (UHV) chamber with a base pressure of

1×10^{-10} Torr. The TPD experiments utilized a UTI 100C mass spectrometer (MS), which was also used for *in situ* verification of the purity of the dosed gases. A Perkin Elmer Auger electron spectrometer (AES) with a cylindrical mirror analyzer was used for surface characterization. An accelerating potential of 3 kV is used for all AES experiments. Polycrystalline W foil (99.95%, Alfa Aesar), measuring 1 mm in thickness, was cut to a diameter of approximately 10 mm resulting in a geometric surface area of 0.998 cm². After cutting, the foil was sonicated in a 50:50 mixture of ethanol and acetone for 1 h. The W foil disk was then spot welded to two tantalum leads so that it could be resistively heated with a DC power supply to 1200 K, or thermally cooled with liquid nitrogen to 100 K. The temperature was measured with a K-type thermocouple spot welded to the back of the W foil disk. Temperature control was achieved by the use of a feedback controller.

Prior to each experiment, the W foil surface was cleaned by several Ne⁺ sputter cycles at 600 K with subsequent flashes to 1050 K. Once clean, the surface was carburized by sputtering in ethylene at 300 K. After the residual ethylene was pumped away, the surface was annealed at 1200 K for 1 min. This resulted in a WC surface with a W:C stoichiometry of 1:1 as verified by AES using standard sensitivity factors. In addition, by performing calculations utilizing the inelastic mean free path of the AES electrons of interest, it was further determined that the surface was predominantly W terminated with perhaps a small fraction of carbon atoms occupying the surface. This is in agreement with results from the characterization of WC(0 0 0 1) [26].

Following carburization, Pt and/or Ni were deposited on the WC surface via physical vapor deposition. The deposition sources consisted of a 0.5-mm-diameter tungsten wire filament wrapped with 0.3-mm-diameter wire of either Pt or Ni. All of the metal wires were purchased from Alfa Aesar and were 99.95+% pure. A DC power supply provided electrical current to resistively heat the filament. During deposition, the temperature of the WC foil was maintained at 300 K. After deposition, the surface was flashed to 600 K to remove carbon monoxide, which was from the adsorption of CO from the UHV background during Ni deposition. To determine the coverage of Ni and Pt, standard overlayer/substrate equations were used in conjunction with tabulated values of the inelastic mean free path (IMFP) of the Auger electrons of interest [27].

$$I_o = I_o^\infty \{1 - \exp[-d_o/\lambda_o(E_o) \cos \theta]\} \tag{1}$$

$$I_s = I_s^\infty \exp[-d_o/\lambda_o(E_s) \cos \theta] \tag{2}$$

$$\frac{I_o}{I_s} = \left(\frac{S_o}{S_s}\right) \frac{1 - \exp[-d_o/\lambda_o(E_o) \cos \theta]}{\exp[-d_o/\lambda_o(E_s) \cos \theta]} \tag{3}$$

In these equations, I_x represents the Auger intensity of element x, with I_x^∞ representing the AES intensity of a bulk slab of element x, S_x is the sensitivity factor of element x, d is the overlayer thickness, $\lambda(E)$ is the IMFP of an electron with energy, E, and θ is the solid acceptance angle of the CMA. It is important to note that the sensitivity factor for tungsten in the carbide phase is not the same as that found in a pure W sample. To account for the difference between this value and that found in the body-centered cubic (BCC) tungsten phase used in the determination of the standard sensitivity factor, an atomic density correction was used. In bulk WC, the atomic density of tungsten is calculated to be 10.82 cm³ mol⁻¹. In comparison, in bulk W, the atomic density is 9.54 cm³ mol⁻¹. Thus, the sensitivity factor of tungsten in WC is 88.2% that of pure tungsten assuming similar values of IMFP in the two materials. Using these equations, the coverage of Ni and Pt for each surface in this study is determined to be ~1.1–1.2 ML for Ni and ~0.6–0.7 ML for Pt. Each metal was deposited at a rate of approximately 0.4–0.5 ML/min.

2.2. TPD measurements

After synthesizing the Pt- and/or Ni-modified WC surfaces, hydrogen (Matheson, 99.999%) and cyclohexene (c-C$_6$H$_{10}$) (Aldrich, 99+%) were dosed at temperatures below 140 K and 130 K, respectively. Cyclohexene was purified by successive freeze–pump–thaw cycles before use. Hydrogen and Ne were of research grade purity (99.999%) and were introduced into the UHV chamber without further purification. Cyclohexene and Ne were backfilled into the chamber through leak valves, while hydrogen was dosed through a directional dosing tube of approximately 8 mm in diameter.

For TPD experiments where only hydrogen was dosed, an exposure of 10 L was used. This amount was sufficient to saturate each surface of interest, with the exception of unmodified WC, which did not saturate until more than 100 L of exposure. Due to the long pumping time of hydrogen, 10 L was dosed on WC despite this amount not resulting in saturation. For the cyclohexene TPD experiments, 0.5 L of H$_2$ was pre-dosed onto each of the surfaces followed by a cyclohexene exposure of 3 L. This amount of cyclohexene provided a small amount of multilayer formation ensuring the saturation of the surface. After dosing, the sample was placed ~5 mm from the opening of the random flux shield of the MS. TPD experiments were then performed with a linear heating rate of 3 K/s, with up to 12 masses being simultaneously monitored.

2.3. DFT calculations

The binding energies of hydrogen and cyclohexene were calculated using the Vienna Ab-initio Simulations Package (VASP). A planewave cutoff energy of 396 eV was used for all calculations using a $3 \times 3 \times 1$ Monkhorst–Pack k-point mesh and the PW91 functional. Spin polarization of both the gas-phase species and the adsorbate-slab system was implemented in these calculations. The base WC(0 0 0 1) slabs were modeled using a 3×3 unit cell with three layers of the (0 0 0 1) WC stacking unit, terminated with W. The next metallic layers (Ni or Pt) were continued using the hcp stacking profile as this was found to be lower in energy than using the fcc sites. The slabs were separated using six to eight equivalent layers of vacuum. The Ni and Pt layers along with the topmost W and C layers of the WC(0 0 0 1) slab were allowed to relax to the lowest energy configuration. The remaining WC layers were fixed at the optimized bulk configuration. The hydrogen binding energy was calculated at a coverage of 1/9 by placing one hydrogen atom at a fcc threefold hollow site, which was found to be more energetically favored compared to the similar hcp threefold hollow site. The cyclohexene binding energy was calculated as bridge bonded

Fig. 1. (a) Top view and (b) side view of example DFT binding orientation for cyclohexene binding on a 3×3 unit cell Pt–Ni–WC(0 0 0 1).

and in the boat configuration as shown in Fig. 1 for Pt–Ni–WC(0 0 0 1). The top two layers were allowed to relax to the lowest energy configuration while the third and fourth layers were frozen at the bulk host metal distance of 2.49 Å for Ni(1 1 1), 2.83 Å for Pt(1 1 1), and 2.95 Å for WC(0 0 0 1), as previously determined for the PW91 exchange/correlation functional. The atomic pseudo-potentials were the ultra-soft Vanderbilt pseudo-potentials as utilized previously [12].

3. Results and discussion

3.1. Surface characterization

Many studies have been conducted to characterize single crystal tungsten substrates modified by Pt or Ni. At room temperature Pt deposition generally proceeds in a layer-by-layer fashion on these substrates, with the possible exception being on the atomically rough W(1 1 1) surface [28–33]. After completion of the second Pt monolayer, it has been shown that a small amount of W diffuses into the Pt layer, even at room temperature. After the layer-by-layer deposition of several monolayers of Pt, three-dimensional growth becomes the dominant growth mechanism. Ni deposition on tungsten single crystals occurs in a much more ideal manner than deposition of Pt, with layer-by-layer growth occurring at room temperature on all single crystal surfaces studied up to the completion of several monolayers [34–38]. Upon annealing these surfaces, however, Ni starts to form three-dimensional islands [38].

While the growth of Pt and Ni on a carburized polycrystalline W surface will likely differ from that seen on single crystal W surfaces, it is useful to compare the results. The AES peak-to-peak heights of Pt (241 eV) and W (182 eV), along with the Pt/W AES ratio, are monitored during Pt deposition on WC foil. As shown in the left panel of Fig. 2, there is a break in the slope of the Pt and W curves after depositing for just under 2 min. It can be argued that there is another break in slightly less than four minutes; however, the break is less clear. To verify that these breaks are indeed due to the completion of Pt monolayers, and thus that layer-by-layer growth occurs for the first two monolayers, Eqs. (1)–(3) are used to determine the Pt/W AES ratio corresponding to the desired Pt coverage. The horizontal dashed line in Fig. 2 corresponds to the Pt/W AES ratio calculated for ~1 ML, which coincides with the breaks in Pt and W intensities indicated by the vertical dashed line. The calculated coverage of Pt with time is plotted in the right panel of Fig. 2. It is seen that there is a linear deposition rate until the completion of ~2 ML, at which point the rate seems to decrease, explaining why the break at ~2 ML coverage is not very clear. The apparent decrease in the deposition rate is explained by one of two phenomena. At higher coverages of Pt, there is either three-dimensional growth or alloying at the Pt–W interface. On W single crystals both were shown to occur, and it is not clear whether that is the case here. The important conclusion is that at monolayer and submonolayer coverages of Pt there is layer-by-layer growth on WC foil.

The growth of Ni, much like on single crystal W substrates, occurs in a layer-by-layer fashion for several monolayers, as demonstrated in Fig. 3. In the left panel, the AES peak-to-peak height of Ni (849 eV) and W (182 eV) and the Ni/W AES ratio are monitored during deposition. Integral monolayers of Ni are seen as breaks in the W and Ni peak-to-peak height, and the Ni/W AES ratio corresponding to 1 ML is verified by overlayer/substrate calculations (horizontal dashed line). The layer-by-layer growth is also verified by the linear increase in the calculated Ni coverage with time as shown in the right panel of Fig. 3. It should be pointed out that the changes in slope in the AES uptake curves (Figs. 2a and 3a) ap-
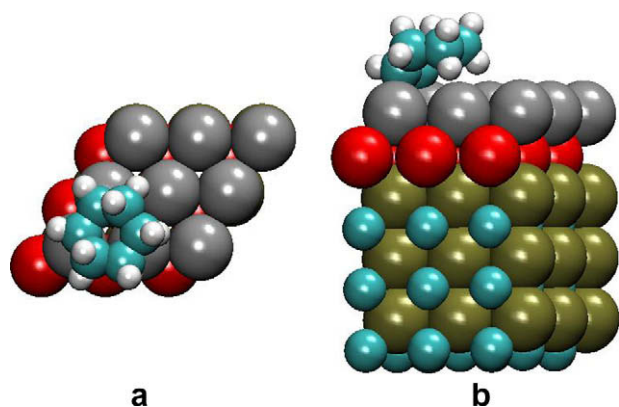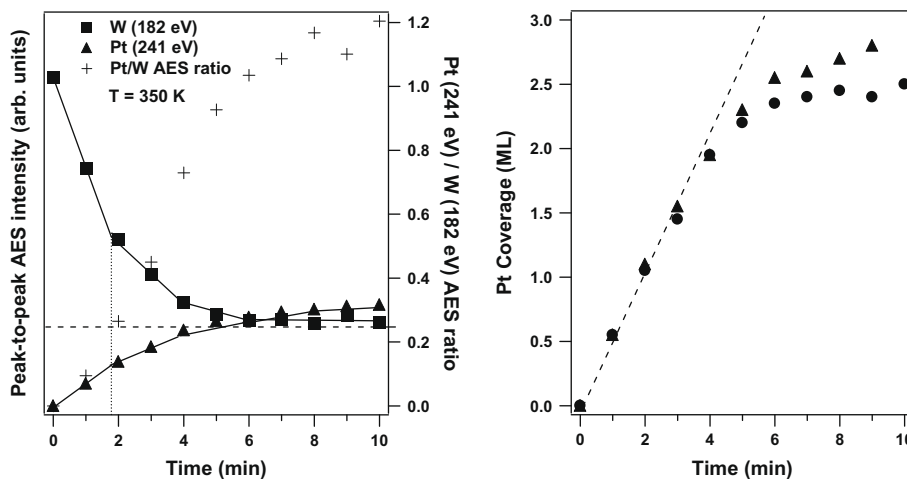
Fig. 2. AES quantification of the physical vapor deposition of Pt on WC foil.
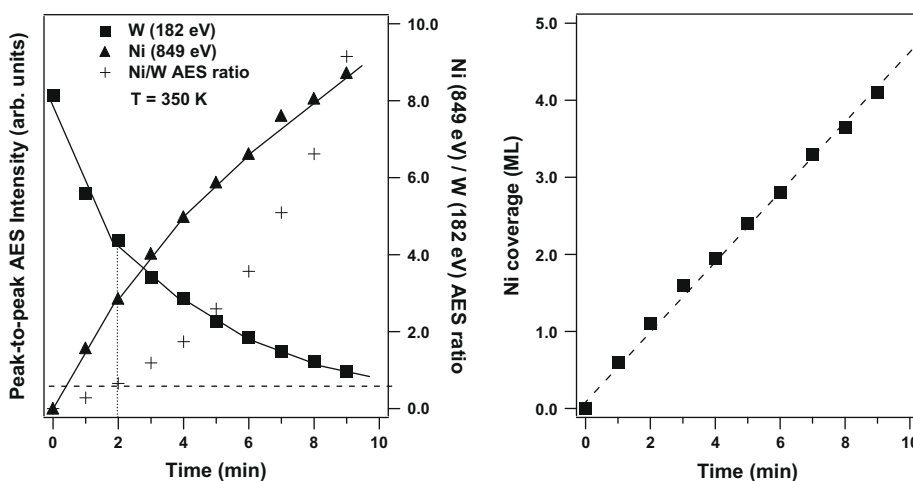

Fig. 3. AES quantification of the physical vapor deposition of Ni on WC foil.

pear to be somewhat subjective. The most important conclusions from the AES results should be the comparisons in Figs. 2b and 3b, which reveal that the growth of the first Pt and Ni layers on WC most likely follow the layer-by-layer mechanism.

In addition to the similarities of Pt and Ni growth on WC foil and W single crystals, the thin films also behave in a similar manner when the respective substrates are annealed. In Fig. 4, it is evident that the Pt/W AES ratio does not significantly change upon annealing a ~1 ML Pt-modified WC surface to temperatures up to 800 K. This is similar to the behavior that was found for ~1 ML Pt on W single crystals. However, it is important to note that upon annealing Pt films thicker than 1 ML on W single crystals, three-dimensional islands formed on top of one monolayer of Pt. In the most extreme case, faceting of the W(1 1 1) surface occurred after annealing to 800–1400 K. This has not been explored in this study as this work is concerned with monolayer and submonolayer Pt coverages, but these phenomena may indeed occur on WC foil for higher coverages of Pt.

Ni/WC, as on single crystal tungsten substrates, appears to agglomerate into three-dimensional islands or clusters upon annealing, as shown in Fig. 4. Initially there is an increase in the Ni/W AES ratio upon heating the surface to 400 K, most likely due to the removal of adsorbed carbon monoxide. However, further increases in temperature cause the Ni/W AES ratio to decrease as islands and clusters begin to form and screen some of the Auger

electrons originating from Ni atoms residing closest to the substrate. The important thing to note is that Ni does not diffuse into the bulk on WC as it does on Pt substrates. This is demonstrated by the fact that upon annealing to temperatures as high as 1000 K (not shown) there is still a significant signal from Ni Auger electrons, with any decreases likely due to screening of the Ni AES electrons by the Ni clusters.

3.2. Hydrogen adsorption

The dissociative adsorption of hydrogen on Pt- and/or Ni-modified WC foil was examined by dosing hydrogen and performing TPD experiments, as shown in Fig. 5. On unmodified WC foil, hydrogen desorbs as a broad peak that is centered at about 311 K. Similar results were seen in a previous study on carbide-modified W(1 1 0), where carburization resulted in a broad hydrogen desorption peak [39]. The breadth of the peak is most likely due to the presence of a variety of surface sites. Due to the polycrystalline nature of the substrate, multiple facets with different crystallographic orientations are present on the surface. In addition, there is a small fraction of surface sites that are carbon-terminated, as suggested by the AES characterization. These different sites should lead to an array of binding environments experienced by the hydrogen atoms. Modification of polycrystalline WC with Pt results in a significant decrease in the hydrogen desorption tem-
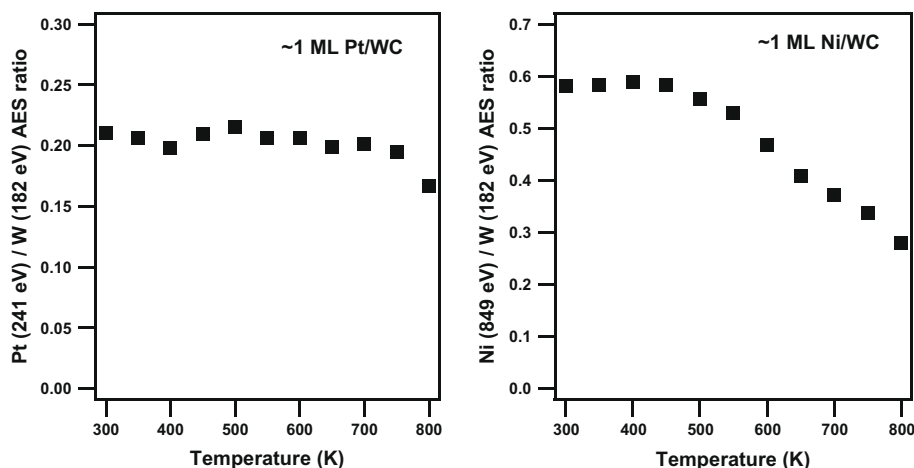
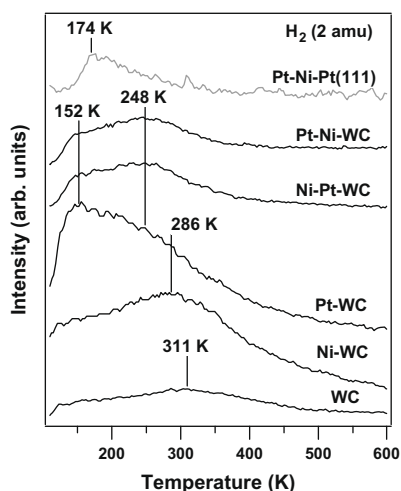**Fig. 4.** AES measurements of the thermal behavior of ~1 ML Pt and Ni on WC foil.

Fig. 5. TPD spectra of hydrogen desorption following the adsorption of 10 L H_2 on Pt- and/or Ni-modified WC foil surfaces.

Table 1
DFT calculations of HBE and cyclohexene BE on Pt–Ni bimetallic surfaces and WC-based surfaces.

	HBE (kJ/mol)	Cyclohexene BE (kJ/mol)
Pt–WC(0 0 0 1)	−61.63	−55.05
Pt–Ni–WC(0 0 0 1)	−88.51	−42.04
Ni–WC(0 0 0 1)	−122.88	−69.91
Ni–Pt–WC(0 0 0 1)	−221.95	−159.18
WC(0 0 0 1)	−200.95	−125.83
Pt–Ni–Pt(1 1 1)	−44.78	−16.13
Ni–Pt–Pt(1 1 1)	−132.33	−73.83
Pt(1 1 1)	−89.58	−66.07
Ni(1 1 1)	−98.49	−24.92

perature, in agreement with previous work on Pt-modified C/W(1 1 0) [39]. It was also found that hydrogen desorption is essentially the same from WC modified by either 0.6 ML or 1.1 ML Pt (not shown) as evidenced by indistinguishable TPD spectra. Based on this observation, and to avoid clustering and alloy formation, all experiments discussed in the current paper use 0.6–0.7 ML of Pt. As shown in Fig. 5, hydrogen desorbs from the ~1.1 ML Ni/WC surface at around 286 K.

Assuming that the dissociative adsorption of hydrogen is unactivated on these surfaces, the temperature of the hydrogen desorption peak is directly related to the binding energy of atomic hydrogen. Thus, the TPD results are in agreement with DFT modeling (Table 1), which predicts that Pt/WC(0 0 0 1) has the weakest hydrogen binding energy, Ni/WC(0 0 0 1) has an intermediate binding strength, and the unmodified WC(0 0 0 1) surface binds hydrogen quite strongly. However, the observation of the relatively broad peaks in the TPD spectra suggests that, despite the general correlation between the hydrogen desorption peak and the hydrogen binding energy, there are also other factors which may affect the bonding of hydrogen on these surfaces.

Of particular interest in the current study are the bimetallic-modified WC surfaces, which are designated as Pt–Ni–WC and Ni–Pt–WC, depending on the order of Pt and Ni deposition. The Pt–Ni–WC surface represents a WC surface onto which Ni is depos-

ited first, followed by Pt deposition. The Ni–Pt–WC surface is synthesized using the reverse deposition order. Hydrogen desorbs from these bimetallic-modified surfaces as two broad peaks at 152 K and 248 K. It is noted that the desorption peak shapes and areas are nearly identical on the two surfaces. This is explained by the fact that they are very similar surfaces due to the fact that, upon flashing to 600 K, Pt migrates to the topmost atomic layer of the Ni–Pt–WC surface to lower the surface energy and strain [25]. In addition, on a vicinal Pt(1 1 1) surface it was found that Ni was able to form an ordered alloy with Pt at temperatures as low as 300 K [40]. Thus, it is likely that there is some exchange between the Pt and Ni layers during deposition prior to the 600 K flash. The effect of deposition order is further investigated by performing consecutive hydrogen TPD experiments on both the Pt–Ni–WC and Ni–Pt–WC surfaces, with each subsequent TPD flashing the surface to increasingly high temperatures up to 800 K. As seen in Fig. 6, the spectra for all of these surfaces are qualitatively similar, with the desorption temperatures being identical and only slight variations in the peak areas. This is an important observation regarding the enhanced thermal stability of Pt–Ni–WC over the Pt–Ni–Pt surfaces. In the latter surface, the annealing causes the diffusion of subsurface Ni to the Pt bulk, therefore, losing the unique chemical properties of the subsurface bimetallic structures.

In order to further understand the enhanced thermal stability of bimetallic structures on WC, Table 2 provides information on the AES quantification of these surfaces. The ratios in this table reflect relative surface atomic concentrations that were calculated using AES peak-to-peak height ratios and standard sensitivity factors. Before discussing the results explicitly, it is important to note that the surface atomic ratios are affected by both clustering and segregation phenomena that are occurring in these experiments, both of
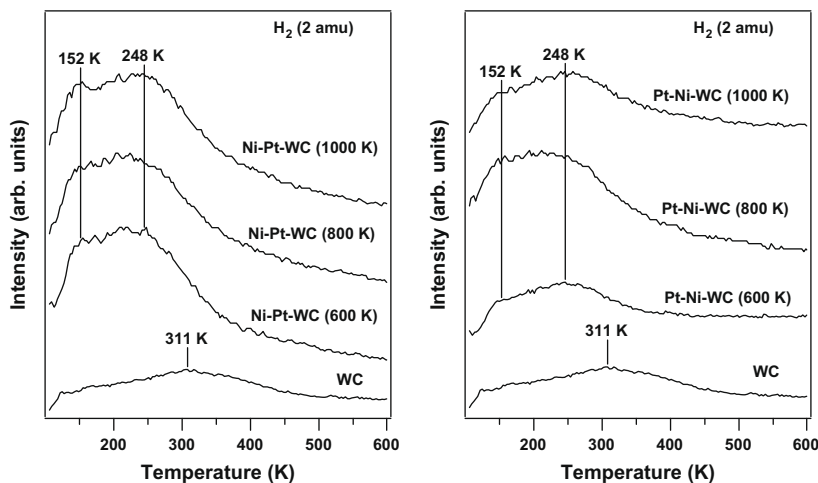
Fig. 6. TPD spectra of hydrogen desorption following the adsorption of 10 L H_2 on Pt- and Ni-modified WC foil surfaces.

Table 2
Effect of deposition order and annealing on the AES ratios of bimetallic-modified WC foil.

Surface	Temperature (K)	Ni/W	Pt/W	Pt/Ni
Pt–Ni–WC	300	0.977	0.219	0.224
Pt–Ni–WC	600	0.852	0.153	0.179
Pt–Ni–WC	800	0.562	0.092	0.164
Ni–Pt–WC	300	1.109	0.211	0.190
Ni–Pt–WC	600	0.943	0.181	0.192
Ni–Pt–WC	800	0.573	0.096	0.167

which can occur simultaneously. The Ni/W and Pt/W atomic ratios decrease with increasing temperature for both the Pt–Ni–WC and Ni–Pt–WC surfaces. As Pt and Ni do not diffuse into WC, this is indicative of cluster formation. In terms of the Pt/Ni atomic ratio, clustering will result in a decrease in this value due to the larger mean free path of Ni (KLL) Auger electrons in comparison with Pt Auger electrons, which results in the Ni Auger electrons being screened to a lesser extent than those of Pt. While this clustering phenomenon is occurring, segregation of Pt to the topmost atomic layer can also occur, resulting in an increase in the surface atomic ratio. Thus, any changes in the Pt/Ni ratio are a direct consequence of the combined effects of these two phenomena. On the Ni–Pt–WC surface, it is apparent that the Pt/Ni ratio remains about the same before and after flashing to 600 K despite thermally induced clustering. Thus, it is concluded that some or all of the Pt atoms migrate to the topmost layer of this surface during the temperature flash. In addition, after the initial deposition at 300 K, the Ni/W and Pt/W AES ratios are comparable for both the Pt–Ni–WC and Ni–Pt–WC surfaces despite the deposition order of Pt and Ni being reversed. Thus, it is indeed likely that exchange between the two atomic layers is occurring, even during deposition. Ultimately, after flashing to each respective temperature the AES ratios of the two surfaces are quite similar, suggesting that deposition order at 300 K is irrelevant in making Pt–Ni–WC. While it is interesting that the Pt/Ni ratio is higher on the Ni–Pt–WC samples flashed to high temperatures, this is most likely due to variations in the amount of Pt being deposited on each of the surfaces. As the amount of Pt used in these studies ranges from 0.6 to 0.7 ML despite identical deposition conditions, one might expect variations in Pt loading up to ~15%.

Like the Ni/WC, Pt/WC, and unmodified WC surfaces, the trend in the desorption temperatures of hydrogen from bimetallic-modified WC surfaces also agrees with DFT results. Specifically, desorp-

tion of hydrogen from Pt–Ni–WC occurs at temperatures between the desorption temperatures from Pt/WC and Ni/WC. In addition, DFT results provide further evidence for the segregation of Pt to the surface. A bimetallic-modified WC surface with Ni on the topmost layer is predicted to bind hydrogen more strongly than WC, and this is certainly not the case for Ni–Pt–WC in Fig. 6, indirectly confirming the segregation of Pt.

An important comparison is that between Pt–Ni–WC (and Ni–Pt–WC) and Pt–Ni–Pt(1 1 1). For hydrogen adsorption, it is seen that the desorption temperatures are very similar between the two surfaces, indicating that the subsurface Pt–Ni bimetallic structure retains its unique chemical properties while anchored on the WC substrate. One relatively minor difference is that the hydrogen desorption peaks are broader on the WC-based surfaces, which may be due to the polycrystallinity of the W foil surface, and any subsequent variations caused by the multiple crystal faces, step edges, and defects.

3.3. Cyclohexene hydrogenation

A novel low temperature hydrogenation pathway of cyclohexene to cyclohexane has been observed on the Pt–Ni–Pt(1 1 1) surface [13,20], and this reaction is used as a probe to compare the chemical properties of the Pt–Ni–WC surfaces to Pt–Ni–Pt(1 1 1). TPD results following the reaction of co-adsorbed hydrogen and cyclohexene are shown in Fig. 7 and the yields of the reaction products are summarized in Table 3. The quantification was performed by calculating the peak areas for benzene (m/z = 78) and cyclohexane (m/z = 84) and scaling these areas to the known yields of these molecules from the Pt–Ni–Pt(1 1 1) surface. As the surface site density is not known for the polycrystalline surfaces, turnover frequencies could not be calculated. Instead, molecular yields normalized to the geometric area of the W foil were calculated and are presented in Table 3. Since Pt–Ni–Pt(1 1 1) is atomically smooth while the WC-based surfaces are polycrystalline and relatively rough, it should be noted that comparisons between yields from the two substrates will have some degree of error.

As the substrate contains a significant amount of carbon and the surfaces are pre-dosed with hydrogen for each TPD experiment, quantification of the decomposition pathway, normally based on the AES measurements of atomic carbon and the TPD peak areas of H_2, is not possible in the current study. Thus, only the yields of gas-phase benzene and cyclohexane on these surfaces will be discussed. A significant amount of cyclohexane and little benzene are produced on the polycrystalline WC surface. The Ni–WC sur-
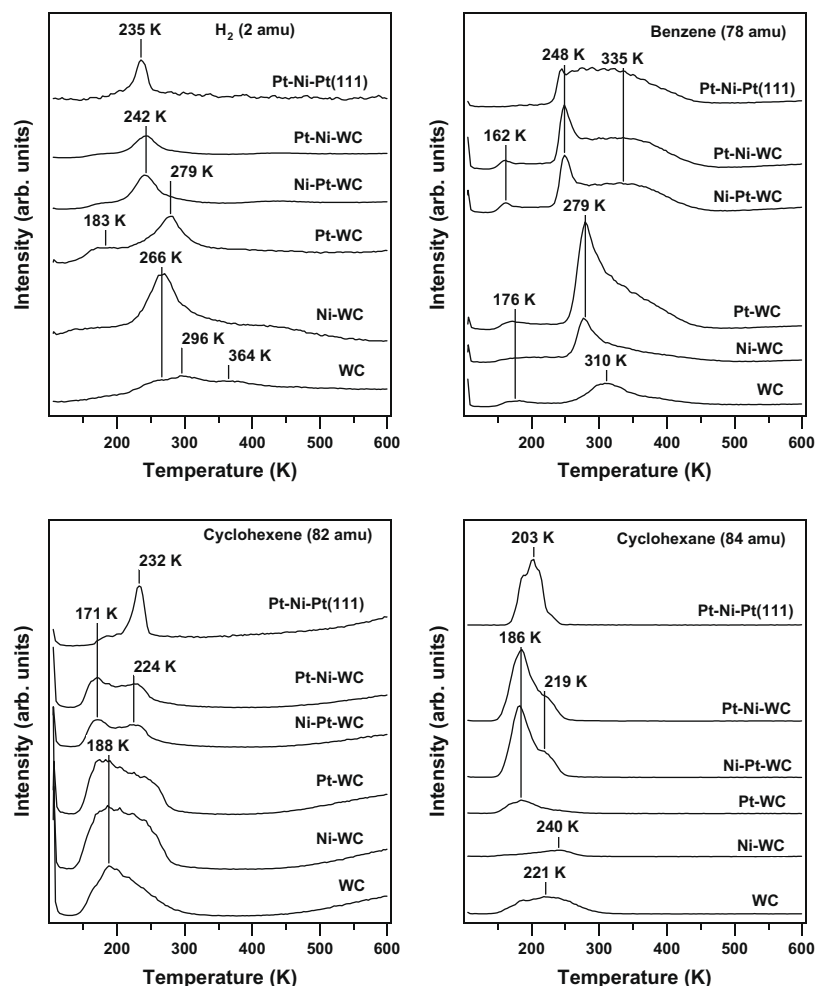
Fig. 7. TPD of cyclohexene on hydrogen pre-dosed Pt- and Ni-modified WC foil surfaces.

Table 3
Cyclohexene hydrogenation and dehydrogenation activities.

Surface	Activity (μmol/m^2)	
	C_6H_6	c-C_6H_{12}
Pt–Ni–Pt(1 1 1)	0.774	0.749
Pt–Ni–Pt foil	0.125	0.954
Pt–Ni–WC	0.743	1.021
Ni–Pt–WC	0.679	0.970
Pt–WC	1.066	0.240
Ni–WC	0.354	0.138
WC	0.254	0.496

face produces a small amount of benzene and a barely detectable amount of cyclohexane. Pt–WC, on the other hand, produces a significant amount of benzene and a very small amount of cyclohexane, similar to the reaction of cyclohexene on the single crystal Pt/C/W(1 1 0) [39,41]. The bimetallic-modified WC surfaces, like Pt–Ni–Pt(1 1 1), produce significant amounts of both benzene and cyclohexane, with a similar yield of cyclohexane being produced on Pt–Ni–WC in comparison with Pt–Ni–Pt(1 1 1). Furthermore, it is seen that the desorption temperatures of these products are similar between Pt–Ni–WC and Pt–Ni–Pt(1 1 1). This is strong evidence that the chemical properties of these two surfaces are similar and that the replacement of bulk Pt in Pt–Ni–Pt(1 1 1), while maintaining desirable catalytic activity and enhanced thermal stability, may indeed be feasible.

While the binding strength and orientation of cyclohexene cannot be determined from TPD experiments, some insight is gained from the DFT calculations of cyclohexene binding energies on different surfaces (Table 1). It was found that cyclohexene bonds to these surfaces though the C=C bond in a boat configuration (shown in Fig. 1). The increased binding of the cyclohexene on the WC supported Pt–Ni surfaces, compared to Pt(1 1 1), is similar to the increased binding seen for other adsorbates (i.e., oxygen, hydrogen, etc.). The increased bonding on WC supported bimetallic surfaces may be due to the combined effect of the increased lattice spacing and the electron density shift away from the surface due to the electron withdrawing WC substrate. This would cause a cascading effect, strengthening general surface bonding with adsorbates.

If arguments consistent with results from studies on Pt(1 1 1) are used [20], one can correlate the hydrogenation activity of a surface with the binding energy of cyclohexene in a volcano-type relationship. As discussed previously on various Pt-based bimetallic surfaces [20], if cyclohexene binds too weakly, it will desorb molecularly before hydrogenation can take place. On the other hand, if cyclohexene binds too strongly, it will lead to the complete decomposition of cyclohexene. Thus, the hydrogenation activity appears to be maximized when there is an intermediate cyclohexene bond strength. This type of volcano relationship is also observed in the current study as illustrated in Fig. 8, with the exception of WC. Based on the binding energy argument alone, it is unclear why there should be a large cyclohexane yield from
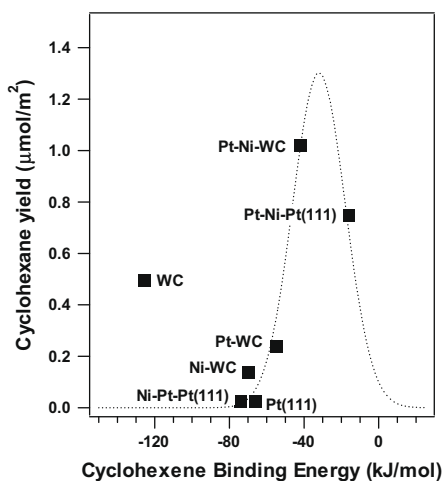
Fig. 8. Correlation of cyclohexane yield with the theoretically determined binding energy of cyclohexene.

WC. Perhaps there is an ensemble effect where sites that bind hydrogen atoms strongly are located near preferred binding sites for cyclohexene. There is also the possibility of some type of defect chemistry occurring, perhaps at a step edge, which would confound a correlation between average surface electronic properties and chemical activity. These ideas are supported by the fact that the single crystal C/W(1 1 0) surface produces a negligible amount of cyclohexane from the hydrogenation of cyclohexene [39]. Despite this outlier, a volcano-type relationship is observed in Fig. 8 and is most likely related to the optimal bonding strength of cyclohexene on the Pt–Ni–WC and Pt–Ni–Pt(1 1 1) surfaces, with weaker bonds favoring molecular desorption and stronger bonds leading to complete decomposition of cyclohexene.

It is important to point out that the surfaces used in the experiment contained multiple facets and step edges. The main purpose of comparing DFT results on the closed-packed facet, such as Pt(1 1 1) or WC(0 0 0 1), to the experimental data is to provide a general correlation between theory and experiments. This assumption would not hold if the chemistry is primarily occurring on the step edges or defect sites as may be the case for bare WC(0 0 0 1). Further studies are necessary to determine the trend of the bare WC(0 0 0 1) surface with experiments. However, results on the Pt–Ni–WC polycrystalline surfaces appear to correlate well with previous studies on the corresponding Pt–Ni–Pt(1 1 1) single crystal surfaces [20].

It is also interesting to point out that, as summarized in Table 3, the bare WC surface exhibits better hydrogenation selectivity, based on the hexane-to-benzene ratio, than the Pt–Ni–WC surface. Although the hydrogenation activity of the WC surface is about 50% less than that of Pt–Ni–WC, the absence of any Pt and better hydrogenation selectivity make the WC surface a potentially attractive hydrogenation catalyst.

4. Conclusions

A combination of surface science experiments and DFT calculations was used to determine the feasibility of replacing the bulk Pt of the Pt–Ni–Pt(1 1 1) bimetallic surface with WC to arrive at a more stable subsurface structure while maintaining its unique chemical properties. The results indicate that the Pt–Ni–WC surface has qualitatively similar chemical activity to the Pt–Ni–Pt(1 1 1) surface while preventing thermal deactivation of the surface to 800 K. Specifically, hydrogen desorbs from both the bimetallic-modified WC and Pt–Ni–Pt(1 1 1) surfaces at a similar temperature. In addition, both surfaces produce a significant yield of cyclohexane from the low temperature hydrogenation of cyclohexene. The results provide strong evidence that it is feasible to replace bulk Pt in Pt–Ni–Pt(1 1 1) with WC, while maintaining desirable catalytic activity and enhanced thermal stability. These results should have important applications in enhancing the activity and stability of Pt-3d subsurface bimetallic structures as hydrogenation catalysts and as cathode electrocatalysts in PEM fuel cells. Because surface oxygen is most likely present on the WC surfaces upon exposing to air, it is important to determine whether tungsten oxycarbide surfaces [41] can be used as a substrate to anchor the Pt–Ni bimetallic structures in future studies.

References

[1] J.H. Sinfelt, Bimetallic Catalysts: Discoveries, Concepts, and Applications, John Wiley & Sons, New York, 1983.
[2] V. Pallassana, M. Neurock, J. Catal. 191 (2000) 301–317.
[3] J.A. Rodriguez, D.W. Goodman, Science 257 (1992) 897–903.
[4] B. Hammer, J.K. Norskov, Adv. Catal. 45 (2000) 71–129.
[5] N.A. Khan, H.H. Hwu, J.G. Chen, J. Catal. 205 (2002) 259–265.
[6] H.H. Hwu, J. Eng Jr., J.G. Chen, J. Am. Chem. Soc. 124 (2002) 702–709.
[7] J.R. Kitchin, J.K. Norskov, M.A. Barteau, J.G. Chen, Phys. Rev. Lett. 93 (2004) 156801.
[8] F. Delbecq, F. Vigne-Maeder, C. Becker, J. Breitbach, K. Wandelt, J. Phys. Chem. C 112 (2008) 555–566.
[9] R. Hirschl, F. Delbecq, P. Sautet, J. Hafner, J. Catal. 217 (2003) 354–366.
[10] J.G. Chen, C.A. Menning, M.B. Zellner, Surf. Sci. Rep. 63 (2008) 201–254.
[11] J.R. Kitchin, N.A. Khan, M.A. Barteau, J.G. Chen, B. Yakshinsiy, T.E. Madey, Surf. Sci. 544 (2003) 295–308.
[12] C.A. Menning, J.G. Chen, J. Chem. Phys 130 (2009) 174709.
[13] M.P. Humbert, L.E. Murillo, J.G. Chen, ChemPhysChem 9 (2008) 1262–1264.
[14] O. Skoplyak, M.A. Barteau, J.G. Chen, Catal. Today 147 (2009) 150–157.
[15] O. Skoplyak, C.A. Menning, M.A. Barteau, J.G. Chen, J. Chem. Phys. 127 (2007) 114707.
[16] C.A. Menning, H.H. Hwu, J.G. Chen, J. Phys. Chem. B 110 (2006) 15471–15477.
[17] L.E. Murillo, A.M. Goda, J.G. Chen, J. Am. Chem. Soc. 129 (2007) 7101–7105.
[18] Y.Y. Shu, L.E. Murillo, J.P. Bosco, W. Huang, A.I. Frenkel, J.G. Chen, Appl. Catal. A – General 339 (2008) 169–179.
[19] S. Lu, W.W. Lonergan, J.P. Bosco, S. Wang, Y. Zhu, Y. Xie, J.G. Chen, J. Catal. 259 (2008) 260–268.
[20] M.P. Humbert, J.G. Chen, J. Catal. 257 (2008) 297–306.
[21] H.H. Hwu, J.G. Chen, Chem. Rev. 105 (2005) 185–212.
[22] S.T. Oyama, The Chemistry of Transition Metal Carbides and Nitrides, Blackie Academic and Professional, Glasgow, 1996.
[23] M.B. Zellner, J.G. Chen, Catal. Today 99 (2005) 299–307.
[24] P. Gouy-Pailler, Y. Pauleau, J. Vac. Sci. Technol. A 11 (1993) 96–102.
[25] C. Creemers, P. Deurinck, Surf. Interface Anal. 25 (1997) 177–190.
[26] J. Brillo, A. Hammoudeh, H. Kuhlenbeck, N. Panagiotides, S. Schwegmann, H. Over, H.J. Freund, J. Electron Spectrosc. 96 (1998) 53–60.
[27] P.J. Cumpson, M.P. Seah, Surf. Interface Anal. 25 (1997) 430–446.
[28] J. Block, J.J. Kolodziej, J.E. Rowe, T.E. Madey, E. Schroder, Thin Solid Films 428 (2003) 47–51.
[29] J. Kolaczkiewicz, E. Bauer, Surf. Sci. 314 (1994) 221–242.
[30] J. Kolaczkiewicz, E. Bauer, Surf. Sci. 374 (1997) 95–103.
[31] J.J. Kolodziej, T.E. Madey, J.W. Keister, J.E. Rowe, Phys. Rev. B 62 (2000) 5150–5162.
[32] J.J. Kolodziej, T.E. Madey, J.W. Keister, J.E. Rowe, Phys. Rev. B 65 (2002) 075413.
[33] C.Z. Dong, S.M. Shivaprasad, K.J. Song, T.E. Madey, J. Chem. Phys. 99 (1993) 9172–9181.
[34] C.Z. Dong, L.Z. Zhang, U. Diebold, T.E. Madey, Surf. Sci. 322 (1995) 221–229.
[35] H.S. Tao, J.E. Rowe, T.E. Madey, Surf. Sci. 407 (1998) L640–L646.
[36] H.L. Meyerheim, D. Sander, R. Popescu, J. Kirschner, O. Robach, S. Ferrer, P. Steadman, Phys. Rev. B 67 (2003) 155422.
[37] C. Schmidthals, D. Sander, A. Enders, J. Kirschner, Surf. Sci. 417 (1998) 361–371.
[38] J. Kolaczkiewicz, E. Bauer, Surf. Sci. 420 (1999) 157–173.
[39] M.B. Zellner, J.G. Chen, J. Catal. 235 (2005) 393–402.
[40] P. Gambardella, K. Kern, Surf. Sci. 475 (2001) L229–L234.
[41] N. Liu, S.A. Rykov, J.G. Chen, Surf. Sci. 487 (2001) 107–117.